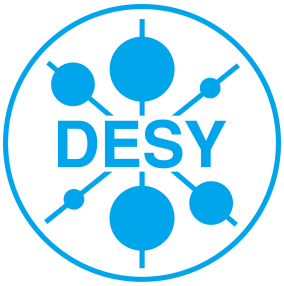

Background reduction in the vector boson fusion produced Higgs $\rightarrow$ invisible search at Atlas using final state photons

Lars Henkelmann, University of Heidelberg, Germany

September 7, 2016

Abstract

The decay of a Higgs boson produced in Vector Boson Fusion into invisible particles has a very low (0.1%) branching ratio in the Standard Model. This makes it an interesting channel to search for new physics in, for example Higgs-Portal dark matter particles. To significantly improve the current upper limit on the $H \rightarrow inv.$ branching ratio of 28%, improving the suppression of background events is crucial. The present report shows how background suppression can be improved by a cut on the highest transverse photon momentum in an event. It is a report on my work in the DESY ATLAS group during the DESY Summer Student Programme 2016.

Contents

1 Introduction **3**
- 1.1 Motivation . . . 3
- 1.2 Observing invisible decays of Higgs bosons . . . 4
  - 1.2.1 Higgs boson production at the LHC . . . 4
  - 1.2.2 Standard model process . . . 5
  - 1.2.3 Background processes . . . 6
- 1.3 Additional final state photons . . . 7

2 Analysis procedure **8**
- 2.1 Samples . . . 8
- 2.2 Cuts . . . 8
- 2.3 Photon requirements . . . 9

3 Results **9**
- 3.1 Jet and missing energy cuts . . . 9
- 3.2 Photon characteristics . . . 12
  - 3.2.1 Photon variables considered for new cuts . . . 13
- 3.3 Transverse photon momentum cut . . . 15

4 Conclusion and Outlook **18**

1 Introduction

1.1 Motivation

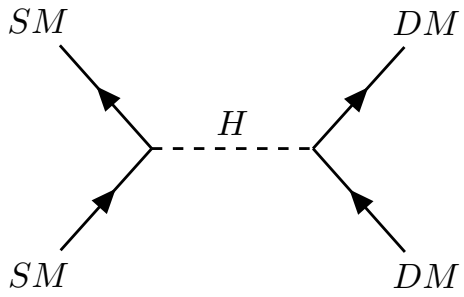

Figure 1: Higgs portal dark matter: the hypothetical interaction of dark matter particles with ordinary matter via Higgs-boson exchange.

There is substantial evidence for the existence of dark matter [1], for example galactic rotation curves [2], the anisotropies of the cosmic microwave background [3], and gravitational lensing [4]. However, dark matter has so far never been observed directly in any laboratory on earth [1].
To detect dark matter directly, it needs to interact with ordinary matter via some interaction other than gravity. One example of such a hypothetical interaction is the exchange of a Higgs boson (Figure 1)[5]. Models where dark matter particles interact with Standard Model particles mainly via Higgs boson exchange are also called "Higgs portal" dark matter models. Higgs portal dark matter can be motivated: by definition, dark matter has mass, and in the Standard Model, all particles acquire mass by interacting with the Higgs field. If dark matter were to acquire mass in the same way, it also would couple to the Higgs boson.
Higgs-portal dark matter can be searched for at particle colliders where Higgs bosons are produced (e.g. the Large Hadron Collider (LHC) at CERN), by looking for Higgs bosons decaying into invisible[1] particles. Such searches are performed by the ATLAS [7] and CMS [8] collaborations. During my stay at DESY I investigated whether the ATLAS vector boson fusion $H \rightarrow inv.$ analysis might be improved by considering additional final state photons.

[1] here, invisible means particles not recorded by the detector

1.2 Observing invisible decays of Higgs bosons

1.2.1 Higgs boson production at the LHC

The main processes for producing Higgs bosons at the LHC, in order of decreasing cross section, are: [6]

- gluon fusion (ggF) (Figure 2)
- vector boson fusion (VBF) (Figure 3)
- associated production processes:
  - WH
  - ZH
  - $t\bar{t}H$
  - $b\bar{b}H$
  - tH

Gluon fusion has the highest cross section for Higgs production [6]. But it cannot be used for a $H \rightarrow inv.$ search, because the entire final state is composed of the Higgs boson itself (Figure 2). If the Higgs boson then decays invisibly, there is nothing left to indicate[2] that a Higgs boson was created in the first place.

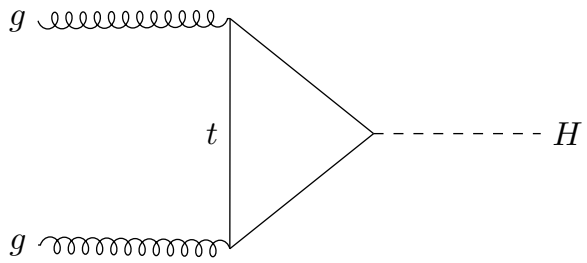

Figure 2: Higgs production via gluon fusion (ggF). Gluon fusion is the dominant Higgs production channel at the LHC [6].

The cross section for producing a Higgs in vector boson fusion is lower [6], but it has a tag: the two quark jets (Figure 3). These jets will typically have high pseudorapidities, transverse momentum, and a large angle between them. The invariant mass of a jet pair from a VBF event will usually also have a large invariant mass. This jet pair and its distinct kinematic signature indicate that vector boson fusion happened in the event, even if there was an invisible decay of a Higgs boson. If a Higgs is produced and decays invisibly, there will likely also be some missing transverse energy.

[2] the gluon fusion channel lacks a so called *tag*

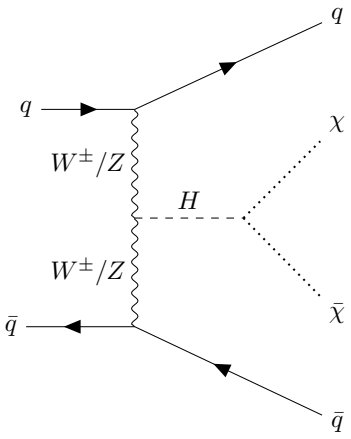

Figure 3: A Higgsi boson produced in vector boson fusion decays into two hypothetical invisible particles. The two quarks in the final state allow identifying events with Higgs even if the Higgs decays invisibly.

1.2.2 Standard model process

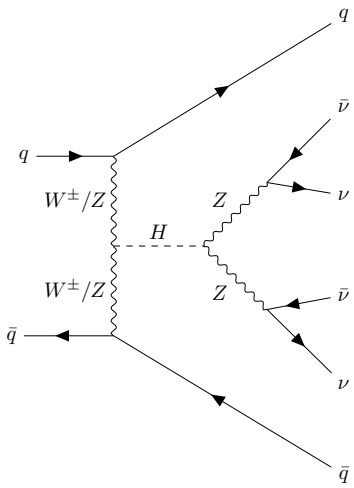

Figure 4: Standard model $H \rightarrow$ *invisible* process. The low branching ratio of about 0.1% [6] means this process is expected to be negligible in the search for invisible Higgs decays.

There is a standard model decay of the Higgs boson which is also invisible to the detector: the decay $H \rightarrow Z^0 Z^0 \rightarrow \nu\bar{\nu}\nu'\bar{\nu}'$ (Figure 4). However the branching ratio of this process is about 0.1% [6], much lower than the current best experimental branching ratio limit of 28% [7]. The standard model signal contribution is therefore entirely negligible.

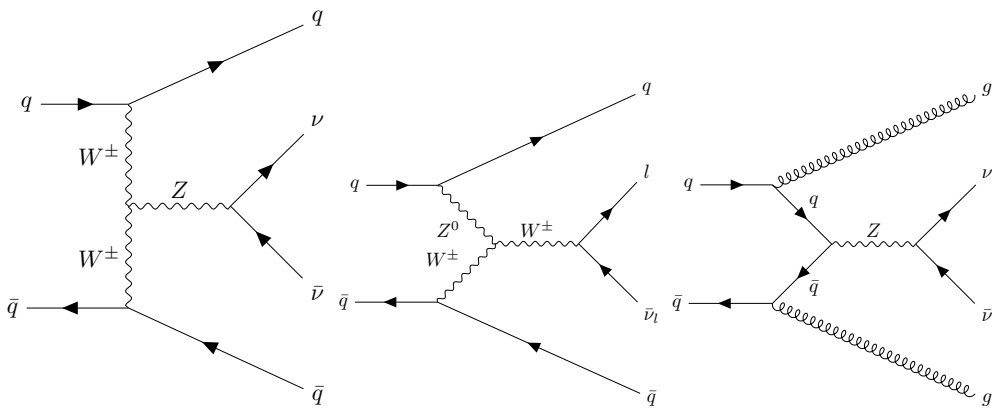

Figure 5: Examples of diagrams contributing to background processes for VBF $H \rightarrow inv.$. (b) can fake an invisible decay if the charged lepton is lost (i.e. recosntructed as part of a jet.)

1.2.3 Background processes

Even though the signal contribution of the standard model invisible Higgs decay (Figure 4) is negligible [6], the background processes are not [7, 8].
There are several processes producing an event topology similar to VBF $H \rightarrow inv.$ that do not produce a Higgs boson: [7, 8]

- VBF $Z^0(\rightarrow \nu\bar{\nu}) + jets$ events (Figure 5a)
- strong scattering events where a $Z^0(\rightarrow \nu\bar{\nu})$ is radiated (QCD $Z^0 + jets$) (Figure 5c)
- VBF $W^{\pm}(\rightarrow l\nu_l) + jets$ events ($l = e, \mu$) where the charged lepton is lost (Figure 5b)
- QCD $W^{\pm} + jets$ events
- multijet events that appear like VBF events due to e.g. misreconstructed E_T^{miss}

There are two steps to dealing with these backgrounds.
First, a set of kinematic cuts (Table 1) is applied to get rid of background events. This strongly suppresses the multijet background. The vector boson fusion backgrounds are difficult to suppress this way, since one does not want to cut away too many potential signal events [7].
In the remaining sample, the number of Z and W background events is estimated using control samples where the vector bosons decay into reconstructed charged leptons. For multijet events, a control sample is constructed from events where the missing energy is aligned with a jet. Finally, a global fit estimates the signal and background yields, and an upper limit on the VBF $H \rightarrow inv.$ branching fraction is set. [7]

Table 1: Selected cuts used to obtain VBF events and reject backgrounds

	observable	cut
VBF signature	$\Delta\eta_{jj}$	> 4.8
–	m_{jj}	$> 1\,\text{TeV}$
multijet suppression	E_T^{miss}	$> 150\,\text{GeV}$
–	$\Delta\phi_{jj}$	< 2.5
–	$\Delta\phi_{j,E_T^{miss}}$	> 1.6 (leading jet) / > 1 (other)

1.3 Additional final state photons

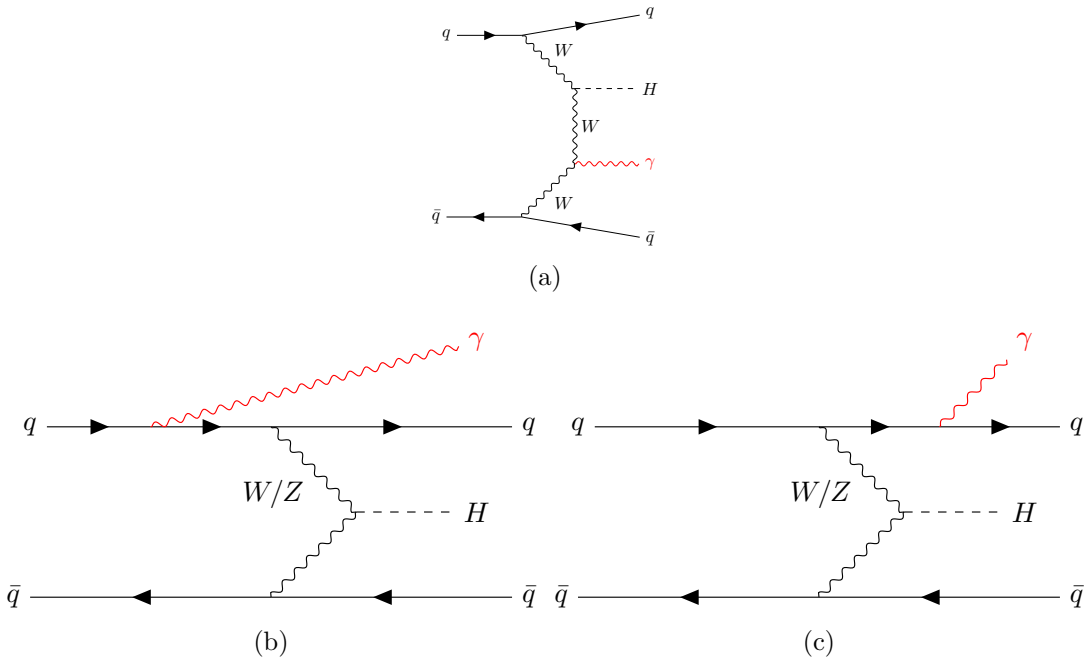

Figure 6: Representative feynman diagrams contributing to VBF $H\ \gamma\ jets$ events.

At first glance, it might seem counterintuitive to consider final state photons to improve the $H \rightarrow inv.$ search. One could expect that requiring an additional photon simply adds one additional QED vertex to all diagrams. The additional vertex, one might think, lowers all cross sections by the same factor of $\alpha = \frac{e^2}{4\pi}$. Were this the only effect, an analysis of events with additional final state photons would be just like the old one, just with smaller samples. Then why should one even consider it?
There exist previous studies of the effect of an additional final state photon on finding Higgs bosons in the $H \rightarrow b\bar{b}$ channel [9], and on the Higgs boson production crosssection [10]. They find that the above simple intuitive expectation of a trivial decrease in sample size falls short. And in [9], the additional photon is shown to improve both the signal significance and the signal to background ratio in identifying $H \rightarrow bb$.

For example, the VBF $H\gamma$ production cross section dominated by W-boson fusion. This is not just because only a charged internal boson line may radiate a photon, as shown in Figure 6a whereas the Z is electrically neutral. The radiation of a central photon by the initial and final state quarks (Figures 6b and 6c) is also supressed. This is because, for Z boson fusion, the diagrams in 6b and 6b interfere destructively (they carry a relative minus sign). But for W fusion, the change of the quark charge due to the charge carried by the W boson leads to an additional relative sign, resulting in constructive interference. The overall effect is that in the VBF production of $H + \gamma$, W fusion contributes about 10 times as much as Z fusion. [9, 10]

2 Analysis procedure

2.1 Samples

Table 2: Monte Carlo samples used in the analysis

Event type	Event Generator	Cross section [pb]
VBF $H(\rightarrow ZZ \rightarrow \nu\bar{\nu}\nu\bar{\nu}) + X$	PowHeg + Pythia8 + EvtGen	3.831
VBF $Z(\rightarrow \nu\bar{\nu}) + X$	Sherpa	13.587
QCD $Z(\rightarrow \nu\bar{\nu}) + X$	Sherpa	11373.0

X contains at least two jets

To determine if and how final state photon properties may help the analysis, the properties of such events are studied using Monte Carlo samples (Table 2). Monte Carlo dijet samples for three types of event are used: VBF Higgs signal samples, VBF Z background samples, and QCD Z background samples.
As a signal sample, an inclusive sample of VBF Higgs events is used (with $m_H = 125\,\text{GeV}$), where the $H \rightarrow ZZ \rightarrow \nu\bar{\nu}\nu\bar{\nu}$ branching fraction is set to 1 (the standard model value is ca. 0.1% [6]).
For both the QCD and the VBF background, only $Z \rightarrow \nu\bar{\nu}$ events, and no $W \rightarrow l\nu$ events are used. This is because the jet kinematics of those two types of event are largely similar. This similarity is a central assumption of the existant analysis [7] where it has been extensively cross-checked.
The Monte Carlo samples do not contain the truth-level event information, but the result of the detector simulation and event reconstruction applied to the truth level particles.

2.2 Cuts

One wants to be sure that the effects of cutting on photon variables are not due to some correlation with the jet kinematics. Therefore the cuts from [7] are reimplemented insofar as they are relevant and applicable here. The cuts used are listed in Table 3. The cut on $\Delta\phi_{j,E_T^{miss}}$ is relaxed for the leading jet (compare Table 1), since multijet background is not considered in the final-state-photon analysis.

Table 3: Cuts on jet kinematics and missing E_T

observable	accept event if
$\Delta\eta_{jj}$	> 4.8
m_{jj}	$> 1\,\text{TeV}$
E_T^{miss}	$> 150\,\text{GeV}$
$\Delta\phi_{jj}$	< 2.5
$\Delta\phi_{j,E_T^{miss}}$	> 1
N_{jets}	$= 2$

2.3 Photon requirements

Since the samples contain reconstructed events, the photons are required to pass certain isolation and identification requirements. Only well isolated photons are considered. The analysis is done for three sets of photons: any particles reconstructed as photons, photon candidates passing an intermediate photon identification requirement, and photon candidates passing a tight identification requirement.
A photon is considered well isolated if the sum of all track momenta found in a cone around the photon track is below a threshold which depends on the photon energy. Also the energy deposited by other particles near the energy deposit of the photon needs to be sufficiently low. A photon isolation requirement based on the presence of jets in a $\Delta R = 0.4$ cone[3] around the photon candidate was also considered. However, there is a strong and nonlinear anticorrelation of $\min_j(\Delta R_{\gamma,j})$ and p_T^γ. Therefore, this isolation requirement is not used.

3 Results

3.1 Jet and missing energy cuts

In the first step, cuts on the jet kinematics and missing transverse energy are implemented, closely following those described in [7](for what is there called "signal region 1").
Figures 7 and 8 show the effect of these cuts on the signal and one background sample. One can see the effect of the cut on the plotted variable, which produces a sharp edge in the distribution. The remaining cuts lead to a mostly uniformly distriubuted decrease in the number of events, hinting at low correlation between the different cut variables. Only the plots for two samples and two cut variables are shown here for the sake of brevity, but the plots for the other samples and variables show the same two features.
Figures 9 and 10 show how the number of accepted events is reduced by each successive cut. Beyond the cuts given in Table 3, increasingly tight photon identification requirements are also shown. The absolute number of events (Figures 9a and 10a) accepted

[3] $\Delta R = \sqrt{\Delta\eta^2 + \Delta\phi^2}$ with pseudorapidity η and azimuthal angle ϕ

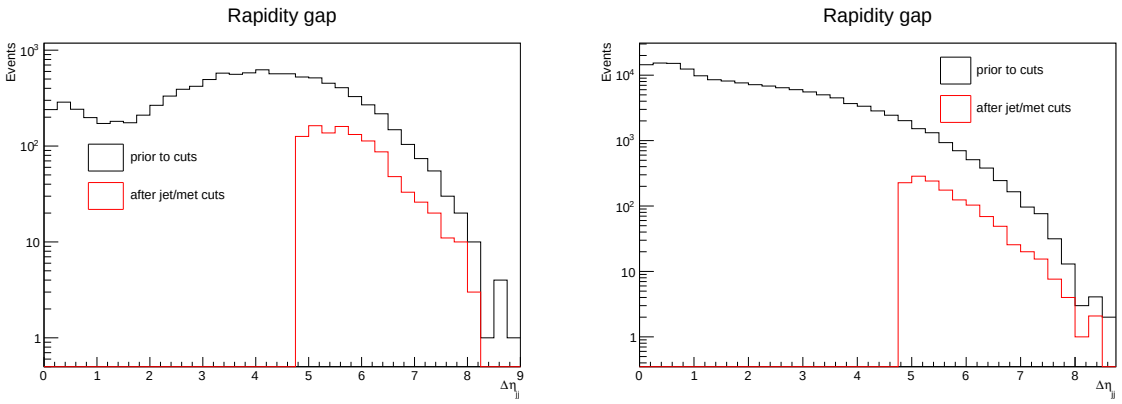

(a) (b)

Figure 7: Effect of the jet and E_T^{miss} cuts (Table 3) on the pseudorapidity gap of the leading and subleading jet of the signal (a) and VBF Z background (b) samples.

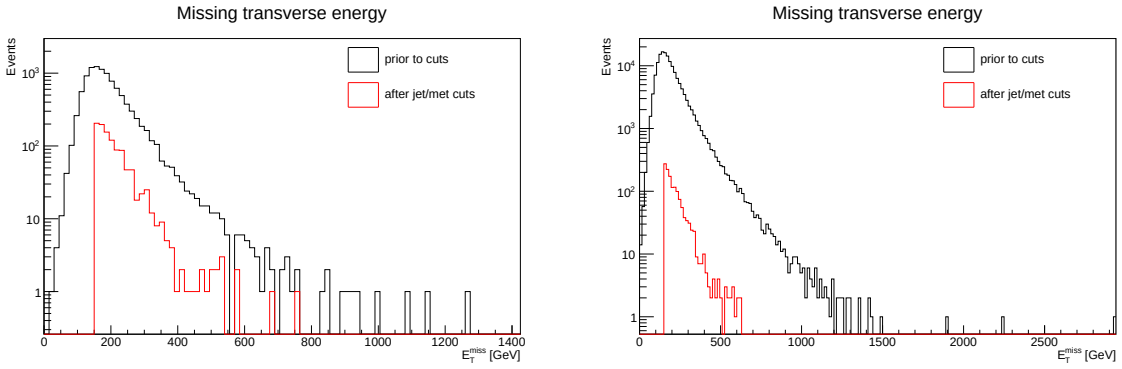

(a) (b)

Figure 8: Effect of the jet and E_T^{miss} cuts (Table 3) on the missing transverse energy distributions of the signal (a) and VBF Z background (b) samples.

in all cuts is comparably small for both samples. But the acceptance for signal events is higher than for background events (Figures 9b and 10b), even though the cuts are designed mainly to reduce multijet background, which is not contained in the VBF Z background sample.

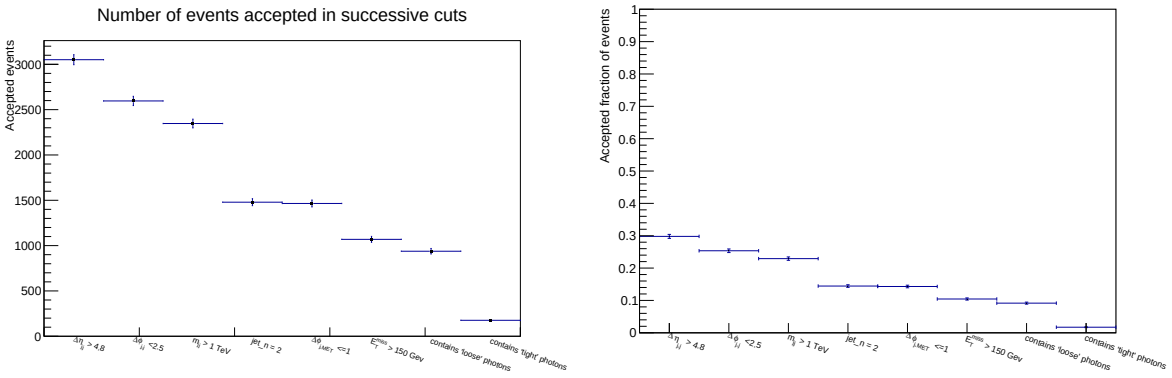

(a) (b)

Figure 9: Effect of the jet and E_T^{miss} cuts (Table 3) and photon requirements applied successively on the absolute (a) and normalized (b) number of accepted signal events.

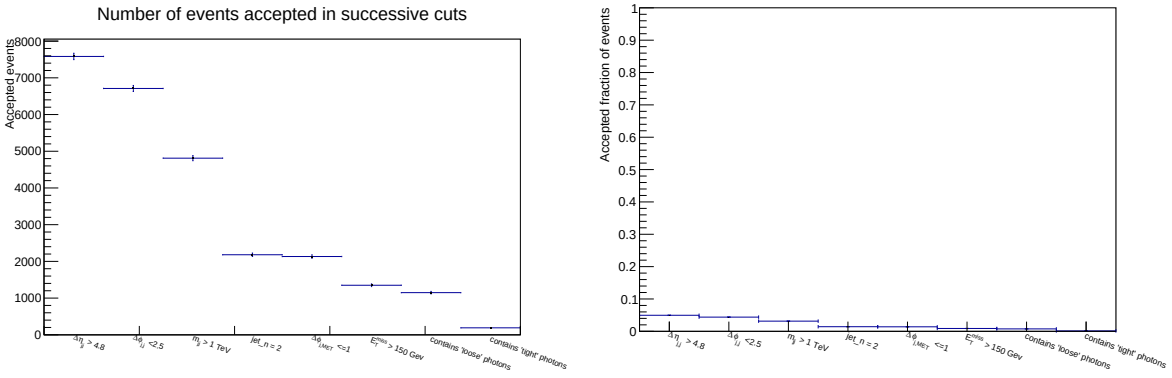

(a) (b)

Figure 10: Effect of the jet and E_T^{miss} cuts (Table 3) and photon requirements applied successively on the absolute (a) and normalized (b) number of accepted VBF Z background events.

3.2 Photon characteristics

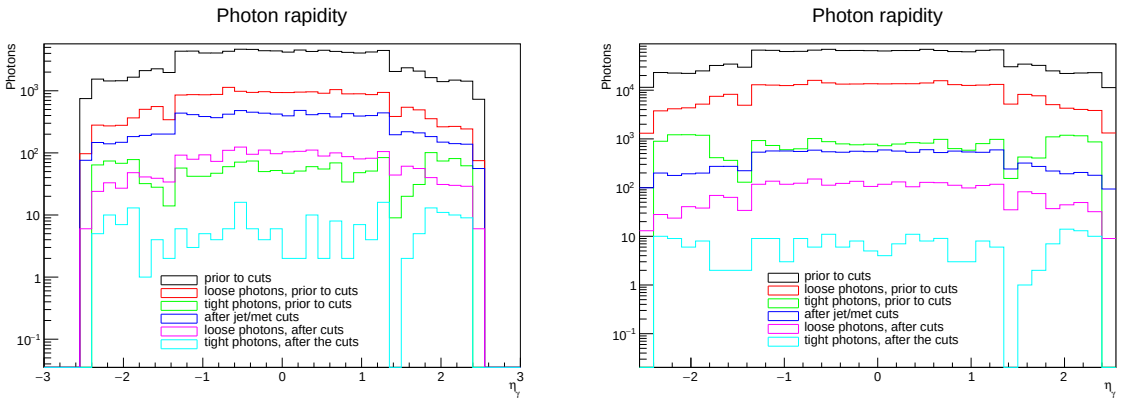

(a) (b)

Figure 11: Photon (pseudo-) rapidity distributions, including all photons of all events in the signal (a) and VBF Z background (b) samples

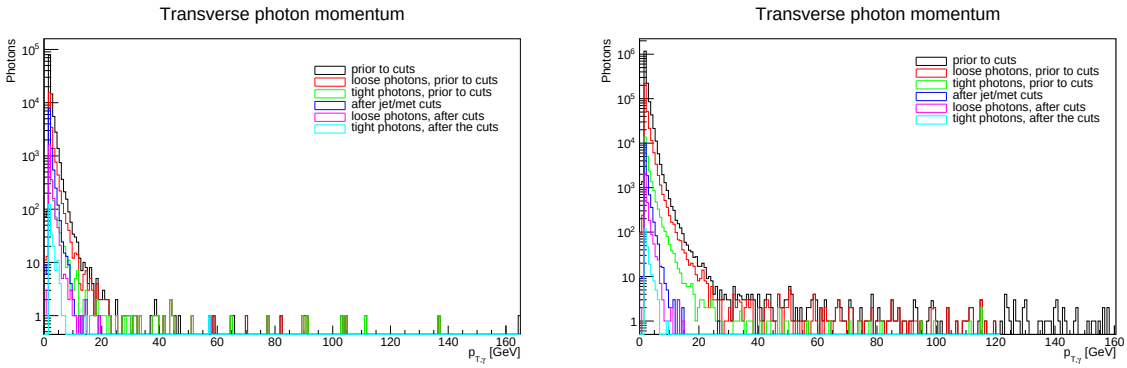

(a) (b)

Figure 12: Transverse photon momentum distributions, including all photons of all events in the signal (a) and VBF Z background (b) samples

The transverse momentum and pseudorapidity distributions of of six different sets of photons are plotted in Figures 11 and 12. There are plots for any photon candidate, candidates passing intermediate identification criteria and candidates passing tight identification criteria. Only well isolated photons are used. The three sets of photon candidates are also plotted for only the subset of candidates in events passing the jet/E_T^{miss} cuts (Table 3).
In Figure 13, the photon candidate multiplicities for the different identification and cut criteria are shown. Many events contain a large number of photon candidates. Most photon candidates have very low transverse momentum. Requiring photon candidiates

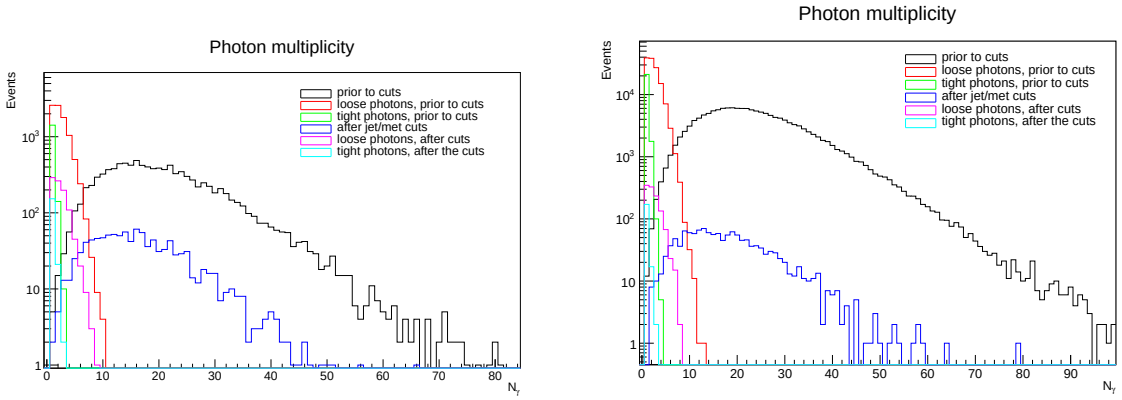

(a) (b)

Figure 13: Photon multiplicity distributions, including all photons of all events in the signal (a) and VBF Z background (b) samples

to pass any of the two identification criteria (medium/tight) strongly reduces both the number of events with any photons, and the number of photons in such events. But even well identified photons have predominantly low transverse momentum. Across all combinations of cut and photon identification requirements, the photon rapidity distribution is mostly uniform within the acceptance of the detector.

3.2.1 Photon variables considered for new cuts

In the search for a suitable photon observable to cut on, a total of 15 variables is considered:

- photon multiplicity: N_γ
- transverse photon momentum: p_T^γ
- photon rapidity: η_γ
- azimuthal photon angle: ϕ_γ
- photon energy: E_γ
- pseudorapidity difference of closest photon-jet pair: $\min_{(j,\gamma)}(\Delta\eta_{j\gamma})$
- R-distance of closest photon-jet pair: $\min_{(j,\gamma)}(\Delta R_{j\gamma})$
- relative azimuthal angle of closest photon-jet pair: $\min_{(j,\gamma)}(\Delta\phi_{j\gamma})$
- pseudorapidity difference of the photon most separated from any jet and its nearest jet neighbour: $\Delta\eta_{\max}$

- R-distance of the photon most separated from any jet and its nearest jet neighbour: ΔR_{max}
- relative azimuthal angle of the photon most separated from any jet and its nearest jet neighbour: $\Delta\phi_{\text{max}}$
- relative azimuthal angle of the $\vec{E}_T^{miss}$ vector and the photon closest to it in the transverse plane: $\max_\gamma(\Delta\phi_{E_T^{miss},\gamma})$
- relative azimuthal angle of the $\vec{E}_T^{miss}$ vector and the photon farthest from it in the transverse plane: $\max_\gamma(\Delta\phi_{E_T^{miss},\gamma})$
- maximum transverse photon momentum: $\max_\gamma(p_T^\gamma)$
- maximum photon energy: $\max_\gamma(E_\gamma)$

The above list of variables is considered seperateley for photons from any event in the MC sample or only photons from events passing the jet and missing E_T cuts. For both of these cases, three different sets of photon candidates are considered: any candidate, only candidates passing the medium tight identification criterion, and only candidates passing the tight selection criterion. So the list of 15 photon variables is checked across 6 different photon samples in total. In each of the 90 variable-sample combinations, the signal, VBF Z background and QCD Z background are independtly normalized to unit area and then overlaid. An example is given in Figure 14. For most of the variables considered, there is no discernible difference in the normalized distributions of signal and background samples (e.g. Figure 14). However, the (maximum) transverse momentum (Figure 15) and (maximum) energy of the photons do show a significant difference. Since photon energy and transverse momentum are expected to be strongly correlated only transverse momentum is discussed in the following.

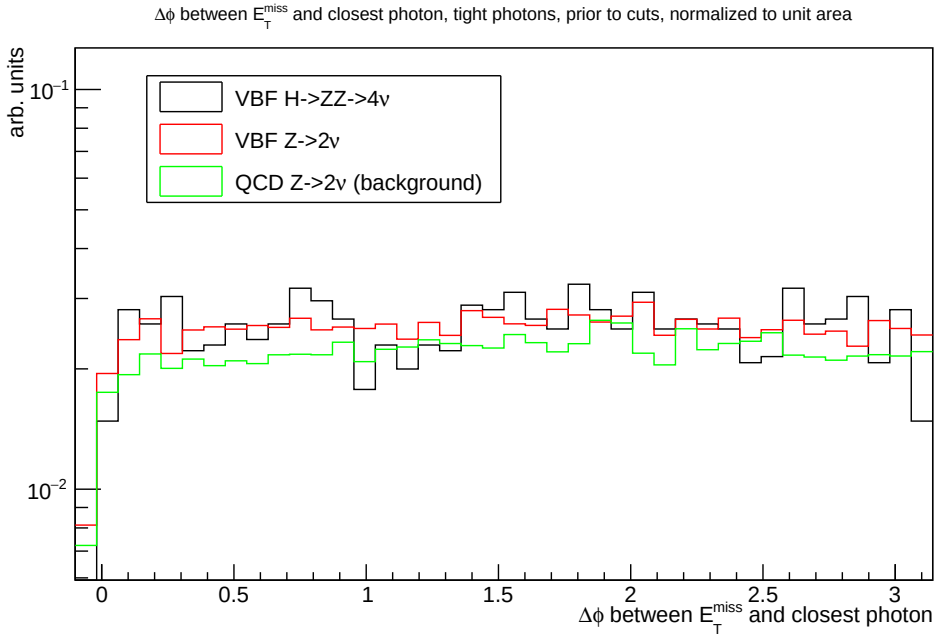

Figure 14: Normalized distributions of the relative azimuthal angle of the $\vec{E}_T^{miss}$ vector and the photon closest to it in the transverse plane, for the signal and the two background samples.

3.3 Transverse photon momentum cut

Figure 15 shows the normalized distributions of maximal signal and background photon p_T. In Figure 15, all events containing at least one well identified and isolated photon are considered. Even events that would be rejected when applying the cuts in Table 3 are included. This is done because otherwise, the total number of signal events with photons would be to small to allow making inferences about the effect of high-p_T^γ cuts on the signal sample. (Figures 9 and 13) The sample including events rejected based on jet/E_T^{miss} cuts on the other hand is large enough to allow statistically significant conclusions (Figure 17). In Figure 16 the efficiencies of accepting signal and background events at different high-p_T^γ cuts are shown. Applying a cut between 10 GeV and 15 GeV means that the probability for a signal event to be accepted is about five times as high as the probability that a background event is accepted. However, the absolute acceptance for signal events is only a few percent in this region. This means that, while in itself there is a point to applying a high-p_T^γ cut, it requires a large data sample in order to have a significant impact on the final result.

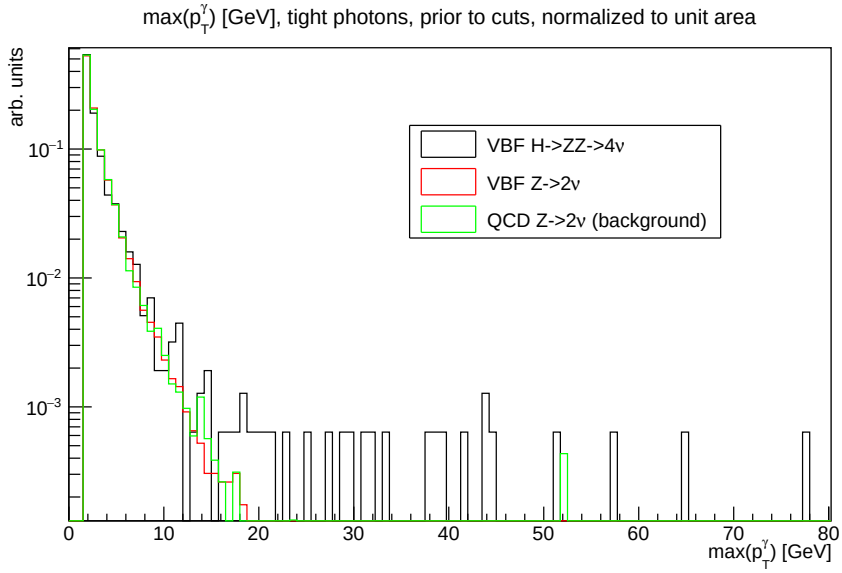

Figure 15: Shape comparison of $\max_\gamma(E_\gamma)$ among signal and background. The two background distributions are very similar. Both differ significantly from the signal distribution.

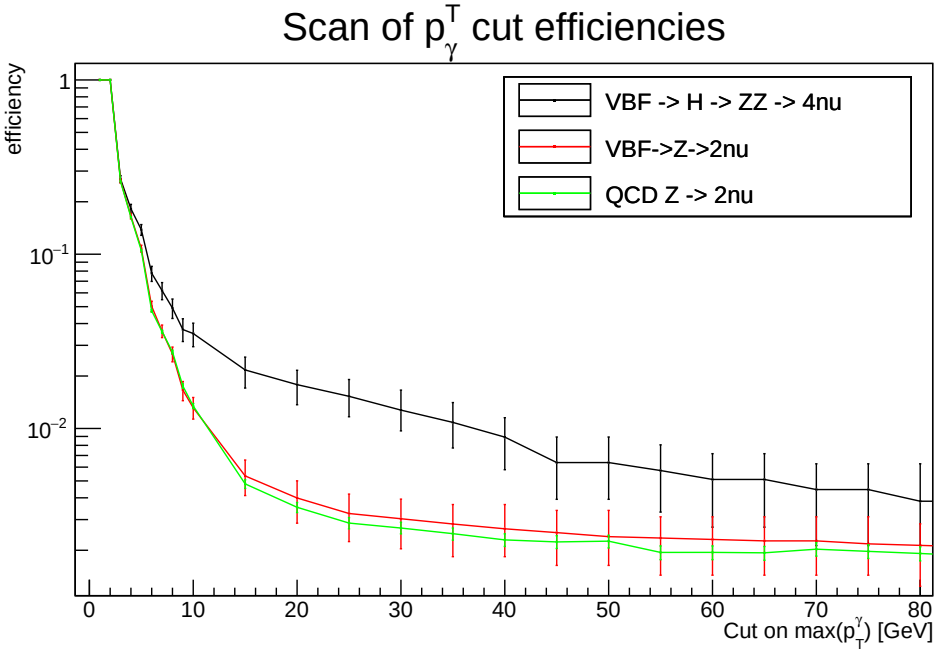

Figure 16: Scan of efficiency (= accepted/total events) across different cuts on $\max_\gamma(E_\gamma)$ for signal and background. The signal acceptance is low, but the background efficiencies are even lower, so a cut can be justified given a sufficiently large data sample. The 1-sigma uncertainty intervals are calculated based on the exact binomial distribution (Clopper-Pearson method [11]).

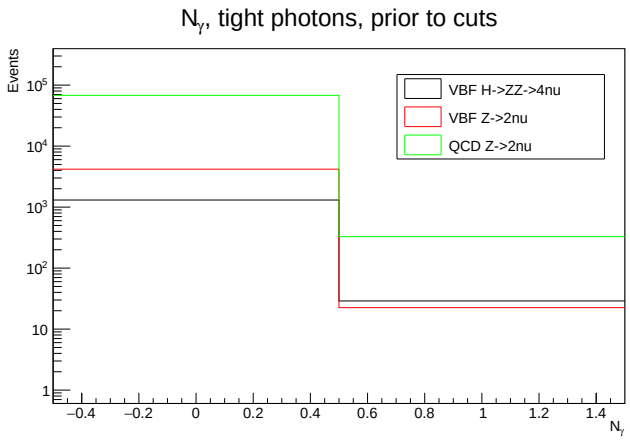

Figure 17: Distribution of the number of photon candidates per event with $p_T^\gamma > 15\,\text{GeV}$. All photon candidates used satisfied tight identifiaction and isolation criteria.

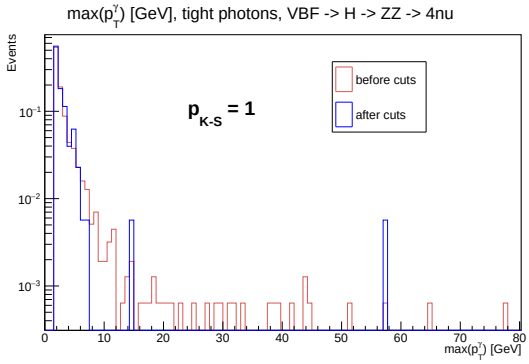

(a)

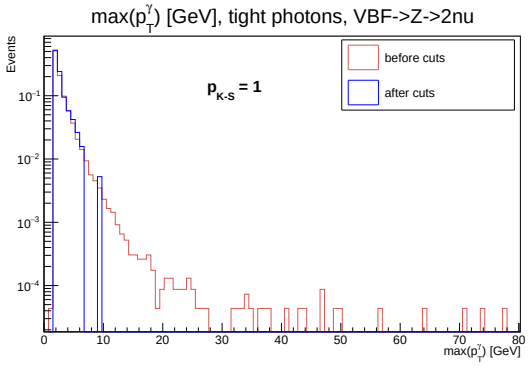

(b)

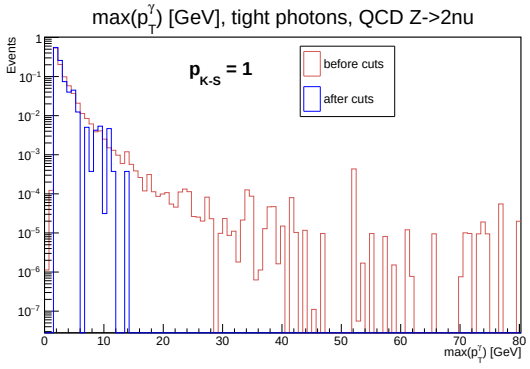

(c)

Figure 18: Comparison of normalized $\max(p_T^\gamma)$ distributions before and after cuts. The comparison is done only for photon candidates passing "tight" identification criteria. The distributions shown are of the signal (a), VBF background (b) and QCD background (c) sample. p_{K-S} is the probability that both distributions originate from the same probability density function, estimated with the Kolmogorov-Smirnov test statistic.

4 Conclusion and Outlook

In conclusion, we found that a cut on the maximal p_T of photons in events can improve the sample purity (Figure 16) in the context of the VBF $H \rightarrow inv.$ search detailed in [7]. However, this cut also strongly reduces the overall sample size. As a result, it is expected to be most useful when applied to large datasets.
There exist several options to improve upon the work reported here. One remaining problem is the low number of events passing the jet and missing E_T cuts (Table 3) and also containg well-isolated, well identified photons. Creating Monte Carlo samples with more events would allow one to check the effect of the photon p_T cut on these events that passed the old cuts. Another interesting check would be to confirm that the particles selected for the cut at reconstruction level are actually, at truth level, photons from the VBF event. In the same vein, it would be interesting to compare the generation procedure of the observed photons across the different Monte Carlo generators used for the signal and background samples (Table 2). This would allow to rule out the possibilty that the effect observed in Figure 16 is due to differences in the photon generation algorithms, and not in the underlying process.

References

[1] G. Bertone, D. Hooper, and J. Silk, *Particle dark matter: evidence, candidates and constraints*, Phys. Rep. **405** 279-390 (2005), doi:10.1016/j.physrep.2004.08.031

[2] Y. Sofue and V. Rubin, *Rotation Curves of Spiral Galaxies*, Annu. Rev. Astron. Astrophys. **39** 137-174 (2001), doi: 10.1146/annurev.astro.39.1.137

[3] S. Dodelson, *Coherent Phase Argument for Inflation*, AIP Conf. Proc. **689** 184 (2003), doi: 10.1063/1.1627736

[4] D. Clowe et. al., *A Direct Empirical Proof of the Existence of Dark Matter*, Astrophys. J. Lett. **648** 109-113 (2006), doi: 10.1086/508162

[5] V. Silveira and A Zee, *Scalar Phantoms*, Phys. Lett. B **161** 136-140 (1985), doi: 10.1016/0370-2693(85)90624-0

[6] S. Dittmaier et.al. (LHC Higgs Cross Section Working Group Collaboration), *Handbook of LHC Higgs Cross Sections: 1. Inclusive Observables* (2011), doi: 10.5170/CERN-2011-002

[7] G. Aad et. al. (ATLAS Collaboration), *Search for invisible Decays of a Higgs boson using vector-boson fusion in pp collisions at* $\sqrt{s} = 8\,TeV$ *with the ATLAS detector*, J. High Energy Phys. **172** (2016), doi: 10.1007/JHEP01(2016)172

[8] S. Chatrchyan et. al. (CMS Collaboration), *Search for invcisible decays of Higgs bosons in the vector boson fusion and associated ZH production modes.*, Eur. Phys. J. C **74** 2980 (2014), doi: 10.1140/epjc/s10052-014-2980-6

[9] E. Gabrielli et. al., *Higgs Boson Production in Association with a Photon in Vector Boson Fusion at the LHC*, Nucl. Phys. B **781** 64-84 (2007), doi: 10.1016/j.nuclphysb.2007.05.010

[10] E. Gabrielli et. al., *Asking for an extra photon in Higgs production at the LHC and beyond*, J. High Energy Phys. **003** (2016), doi: 10.1007/JHEP07(2016)003

[11] C. J. Clopper and E. S. Pearson, *THE USE OF CONFIDENCE OR FIDUCIAL LIMITS ILLUSTRATED IN THE CASE OF THE BINOMIAL*, Biometrika **26** (4) 404-413 (1934), doi: 10.1093/biomet/26.4.404

Acknowledgements

I would like to thank my supervisors Alexander Madsen and Kristzian Peters for their advice, help and feedback during my summerstudent project, as well as the ATLAS team at DESY. I am grateful towards the DESY summerstudent team for organizing the DESY Summerstudent Programme in 2016.